Challenge Journal of Concrete Research Letters

Research Article

Performance of light weight ferrocement composite walls

Yousry B. I. Shaheen [a], Zeinab A. Etman [a], Doha E. A. Kandil [a,*]

[a] *Department of Civil Engineering, Menoufia University, Shebin ElKoum, Menofia, Egypt*

ABSTRACT

The aim of this research is to examine the performance of reinforced lightweight ferrocement walls under vertical and horizontal loading. The walls were made up of two thin layers of ferrocement reinforced with one, two, three, or four layers of welded wire mesh or expanded steel mesh. The panels' core was constructed of lightweight extruded foam. An experimental program of thirteen lightweight walls with total dimensions of 100x650x1250 mm was casted to achieve this goal and tested until failure. ABAQUS finite-element package was conducted. The parameters in this study were the kind of reinforcement; welded and expanded wire meshes, the steel bars, and. the number of layers of steel mesh. Ultimate load, mode of failure, initial cracking load, service load, energy absorption, and ductility ratio were calculated and observation to evaluate the findings. The findings displayed that the performance of the ferrocement walls reinforced with expanded wire meshes is better than that of the walls reinforced with welded wire meshes. The energy absorbed increased by 40 % for specimens reinforced with expanded wire meshes is more than that of the walls reinforced with welded wire a good agreement was observed among the theoretical and experimental observations. This paper highlights uses of employing light weight ferrocement units in building of economic housing, which is particularly valuable for both developed and developing nations, with significant frugal benefits.

ARTICLE INFO

Article history:
Received 29 April 2023
Revised 7 June 2023
Accepted 5 July 2023

Keywords:
Ferrocement
Welded mesh
Expanded mesh
Composite walls
Finite element method
ABAQUS

1. Introduction

Ferrocement is a composite material made up of a mortar matrix and a number of layers of steel mesh reinforcement embedded in the matrix. Shaheen et al. (2017) described a novel precast U-shape ferrocement form reinforced with metallic and non-metallic mesh reinforcement. The experimental program compares casting and testing ten slabs with total dimensions of 500x100x2500 mm that include 40 mm thick U shape permanent ferrocement forms. The testing program revealed that the suggested slabs could achieve high ultimate and serviceability loads, superior fracture resistance management, high ductility, and strong energy absorption qualities at a reasonable cost when compared to the control specimen.

Shaheen et al. (2021) assessed the experimental and theoretical calculation of ferrocement walls. Under concentric compressive stresses, twelve RC walls with dimensions of 450 mm x 100 mm x 1000 mm were tested. The factors under consideration include material k of reinforcing, the number of mesh layers, and the volume fraction of the reinforcement. The study's goal is to evaluate the effect of employing new revolutionary materials in reinforcing RC composite walls. Nonlinear analysis was used to emulate the behavior of tested specimens using the ANSYS-10.0 software. The parametric research is also explained in detail in order to investigate alterations that can be expect with different results with more variable, such as modifying the wall dimensions. The numerical findings obtained revealed that the FE simulation had an adequate accuracy in approximating the experimental values. Furthermore, the strength acquired by samples reinforced with welded steel mesh was 40% greater than that gained by those reinforced with expanded steel mesh. In comparison to ordinary reinforced concrete specimens, ferrocement specimens evaluated under axial compressive stresses demonstrate better ultimate loads and energy absorption capacity.

* *Corresponding author*. Tel.: +2-01-021-372820 ; E-mail address: engdohakandil@gmail.com (D. E. A. Kandil)
ISSN: 2548-0928 / DOI: https://doi.org/10.20528/cjcrl.2023.03.002

Shaheen et al. (2018) examined the performance of precast lightweight ferrocement walls and ANSYS14.5 was used as finite element package. The precast lightweight ferrocement hollow blocks of 200*400*200mm and filled with the core material the core material was hollow blocks. These blocks were arranged to form four walls that measured 840*650*250mm. The core material was investigated as one layer of welded steel mesh. Welded steel mesh was used as a bonding layer form to support the plastering in single, double, and three layers. The results show that the experimental results confirmed that better cracks resistance, high serviceability and ultimate loads, and good energy absorption could be improved using the proposed walls which verify the validity of used the proposed model.

Shaheen et al. (2019) examined the structural behavior of thin ferrocement plates exposed to axial compression loads with and without a frame. The theoretical model ANSYS15 was used. Twelve samples of 50 mm thick, 1000 mm wide, and 1000 mm long thin ferrocement plates were tested under compression stress till failure.

With particular attention devoted to first cracking, maximum load, deflection at different stages of loading, fracture pattern, energy absorption, and ductility index, the behavior of the tested thin plates was assessed. As well as increased deformation qualities, high strength, ductility, and energy absorption, a test specimen reinforced with three layers of welded steel wire steel meshes combined with seven steel bars as steel reinforcement (FS7W3) also showed these properties. A good agreement between the theoretical and experimental finds.

Shaheen et al. (2021) inspected the structural performance integrity of lightweight semicircular ferrocement composite roof panels. The suggested panels weight less than conventional reinforced concrete panels. Two thin layers of ferrocement reinforced with one or two layers of welded wire mesh closely together made up the sandwich panels. The core was constructed from low weight fibrous foam concrete. Shear was transferred among the two layer of ferrocement skin layers via the core in-between using steel wires from the two skin layers that were employed to connect the steel meshes and serve as shear connectors.

The skin of the ferrocement will be 25 mm thick. The core material, which will be 70 mm thick and made of pyrite and ad pour 55 as lightweight aggregate, will be 70 mm thick. To strengthen the skin, two types of steel mesh were employed. Welded wire mesh and expanded metal mesh are two examples. Steel wire shear connectors will be utilized to link the top and bottom skin layers, and also provide shear reinforcement. The panels were subjected to experimental testing. A total of 16 sandwich semicircular panels with dimensions of 500 mm in width and 2000 mm in length were tested up to failure under four lines loadings of span 1900 mm. the behavior of each panel in deformation and cracking were recorded and monitored. The final observation will be compared to theoretical ones using the ABAQUS finite elements software version 14. The findings will indicate that the suggested panels can achieve high ultimate and serviceability loads, fracture resistance management, a high ductility ratio, and superior energy absorption qualities.

Shaheen et al. (2022) studied the properties of lightweight ferrocement walls. The results show that the walls with expanded mesh had more ultimate load compared with walls reinforced with welded mesh.

Shaheen et al. (2023) examined the flexural behavior of ferrocement beam. They used fourteen beams with dimensions (1000, 100 and 150 mm) reinforced with welded and expanded meshes. All beams tested till failure under flexural load. They observed that ferrocement beams achieved high ultimate and serviceability loads, crack resistance, high ductility.

In this research we searched the performance of ferrocement walls under two loads (compressive and lateral) with core material as foam. On the other hand, the previous studies discussed the effect of one direction loading and some other core material like hollow block.

2. Research Significance

This work depicts light weight ferrocement walls that have been exposed to uniform axial compression and lateral loadings. As an alternative to traditional reinforcement, welded steel wire and extended steel wire networks are utilized. The essential goals of the experimental program detailed in this think about were to:

- Examine the performance of light weight ferrocement composite walls under uniform axial compression and lateral loadings.
- Investigating the influence of reinforcing kind and number of layers of steel wire meshes (one, two, three, and four layers.) on performance of ferrocement walls. ABAQUS, finite element tool, will undertake theoretical analysis to validate the experimental program's results.

3. Material Properties

Throughout the current study:

Aggregate sand was employed as the fine aggregate. Table 1 displays the results of a sieve analysis performed on the sand used in the ferrocement mortar mix.

CEMI 42.5 N was utilized, and its mechanical and physical qualities were examined for concrete works in accordance with E.S.S, 4756-11 (2013).

The water utilized for mixing and curing the examined specimens was pure drinking fresh water devoid of contaminants.

Polypropylene 300–e3 fibers were utilized. It was offered in Egyptian stores. It was employed in concrete mixtures to improve the properties of the concrete. Based on manufacturer guidelines, the proportion of increment was set at 900 gm/m^3. Table2 shows the properties of Polypropylene fibers 300-e3

A high range water reducer HRWR was employed as a super plasticizer. It was employed to increase the mix's workability. Sika Egypt provided it for Construction Chemicals in the concrete mix of walls. It satisfies the su-

per plasticizer criteria of ASTM-C-494 Types G and F and BS EN 934 Part 2: 2001.

Silica fume powder with a grey tint was utilized to replace some of the cement. Silica fume was employed to exchange 10% of the cement composition by weight. Table 3 displays the properties of silica fume.

Steel reinforcement as reinforcing bar, mild steel 8 mm in diameter was employed.

Expanded metal mesh was used to strengthen ferrocement channels. The weight of expanded wire mesh per m^2 was 1500 gm.

The galvanized welded metal mesh utilized in this project was acquired from China. As reinforcement for ferrocement channels, welded metal mesh was employed. The m^2 of welded weir mesh was recorded 450 gm in weight.

Foam is a blue board (1.25x0.6x0.5 m) created using a continuous extrusion technique, with unique qualities such as low thermal conductivity, strong resistance to water penetration, high compressive strength, and a density of 36.5 kg/m^3.

Table 1. Results of the sieve analysis for fine aggregates.

Sieve diameter (mm)	4.75	2.83	1.41	0.707	0.354	0.177
Pass (%)	97.7	89.7	67.5	49	3.8	1.6

Table 2. Properties of Fiber mesh 300–e3.

Absorption	Nil
Specific gravity	0.91 gm/cm3
Fiber length	Single cut lengths
Electrical conductivity	Low
Acid and salt resistance	High
Melt point	324°F (162°C)
Thermal conductivity	Low
Ignition point	1100°F (593°C)
Alkali resistance	Alkali proof

Table 3. Chemical composition of silica fume.

Chemical	SiO_2	C	Fe_2O_2	CaO	Al_2O_2	MgO	MnO	K_2O	Na_2O
Weight (%)	92-94	3-5	0.1-0.5	0.1-0.15	0.2-0.3	0.1-0.2	0.008	0.1	0.1

4. Experimental Program

The experiment was carried out on thirteen walls. All test specimens had the same concrete proportions, with a total height of 1250 mm and cross sectional dimensions of 100x650 mm. Table 4 includes information on the test specimens. The specimens was designed by code, CO for the control wall which reinforced with steel bars, while the code W respect the wall reinforced with welded mesh, as well as the code WS for walls reinforced with welded mesh with steel bar, E the code of walls which reinforced by expanded mesh, moreover the code ES were reinforced by expanded mesh with steel bar. In addition, the number refers to the count of the layer.

Table 4. Details of the test specimens.

Name	Type	Description
CO	Control	4 Φ 8 m
W2	Welded mesh	2 layer u & b
W3		3layer u & b
W4		4layer u & b
WS2	Welded mesh with steel bars	2layer u & b &4 Φ 8
WS3		3layer u & b & 4 Φ 8
WS4		4layer u & b & 4 Φ 8
E1	Expanded mesh	1layer u & b
E2		2layer u & b
E3		3layer u & b
ES1	Expanded mesh with steel bars `	1layer u & b & 4 Φ 8
ES2		2layer u & b & 4 Φ 8
ES3		3layer u & b & 4 Φ 8

4.1. Reinforcement details

The following figures showing the reinforcement details of all specimens in Figs. 1-5.

4.1.1. Reinforcement details of control wall (CO)

This group consist of the control wall. This wall was reinforced with four mild steel bars of 8 mm diameter in each side 4Ø8mm as shown in Fig. 1.

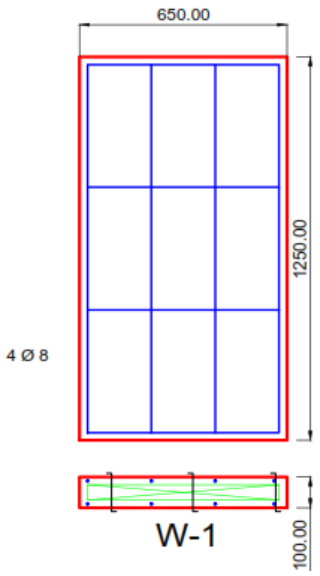

Fig. 1. Reinforcement details of control wall (CO).

4.1.2. Reinforcement details of Group-1 walls (W2, W3 and W4)

This group consist of three walls. The walls in this group are reinforced with welded steel mesh as well as W2 reinforced with two layer of welded steel mesh in each side, W3 reinforced with three layer of welded steel mesh in each side, and W4 reinforced with four layer of welded steel mesh in each side as shown in Fig. 2.

4.1.3. Reinforcement details of Group-2 walls (WS2, WS3 and WS4)

This group consist of three walls. The walls in this group were reinforced with welded steel mesh with steel bar as well as WS2 reinforced with two layer of welded steel mesh plus 4 Φ 8 in each side, WS3 reinforced with three layer of welded steel mesh plus 4 Φ 8 in each side and WS4 reinforced with four layer of welded steel mesh plus 4 Φ 8 in each side as shown in Fig. 3.

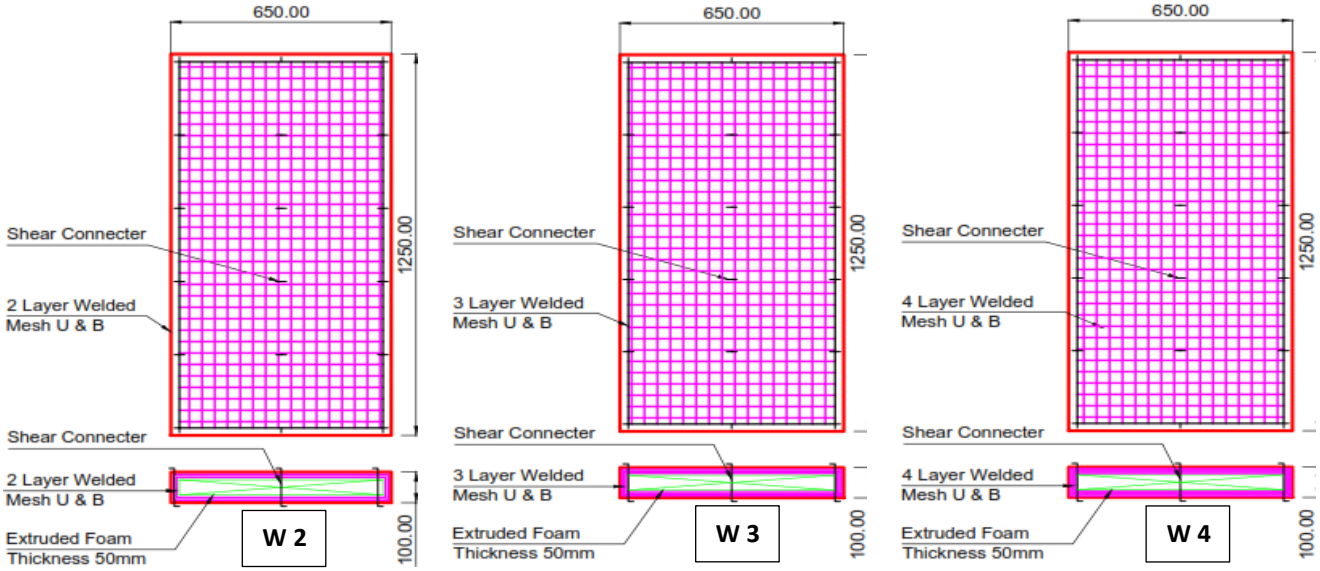

Fig. 2. Reinforcement details of Group-1 walls (W2, W3 and W4).

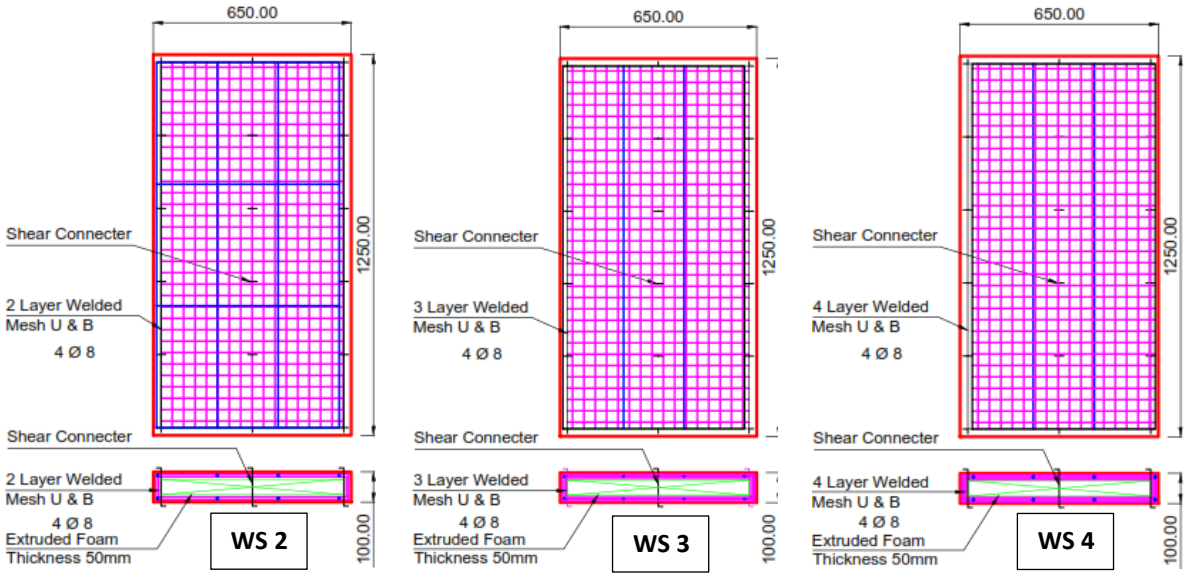

Fig. 3. Reinforcement details of Group-2 walls (W2, W3 and W4).

4.1.4. Reinforcement details of Group-3 walls (E1, E2 and E3)

This group consist of three walls. The walls in this group were reinforced with expanded steel mesh as well as E1 reinforced with one layer of expanded steel mesh in each side, E2 reinforced with two layers of expanded steel mesh in each side and E3 reinforced with three layers of expanded steel mesh in each side as shown in Fig. 4.

4.1.5. Reinforcement details of Group-4 walls (ES1, ES2 and ES3)

This group consist of three walls. The walls in this group are reinforced with expanded steel mesh with steel bars as well as ES1 reinforced with one layer of expanded steel mesh plus 4 Φ 8 in each side, ES2 reinforced with two layers of expanded steel mesh plus 4 Φ 8 in each side and ES3 reinforced with three layers of expanded steel mesh plus 4 Φ 8 in each side as shown in Fig. 5.

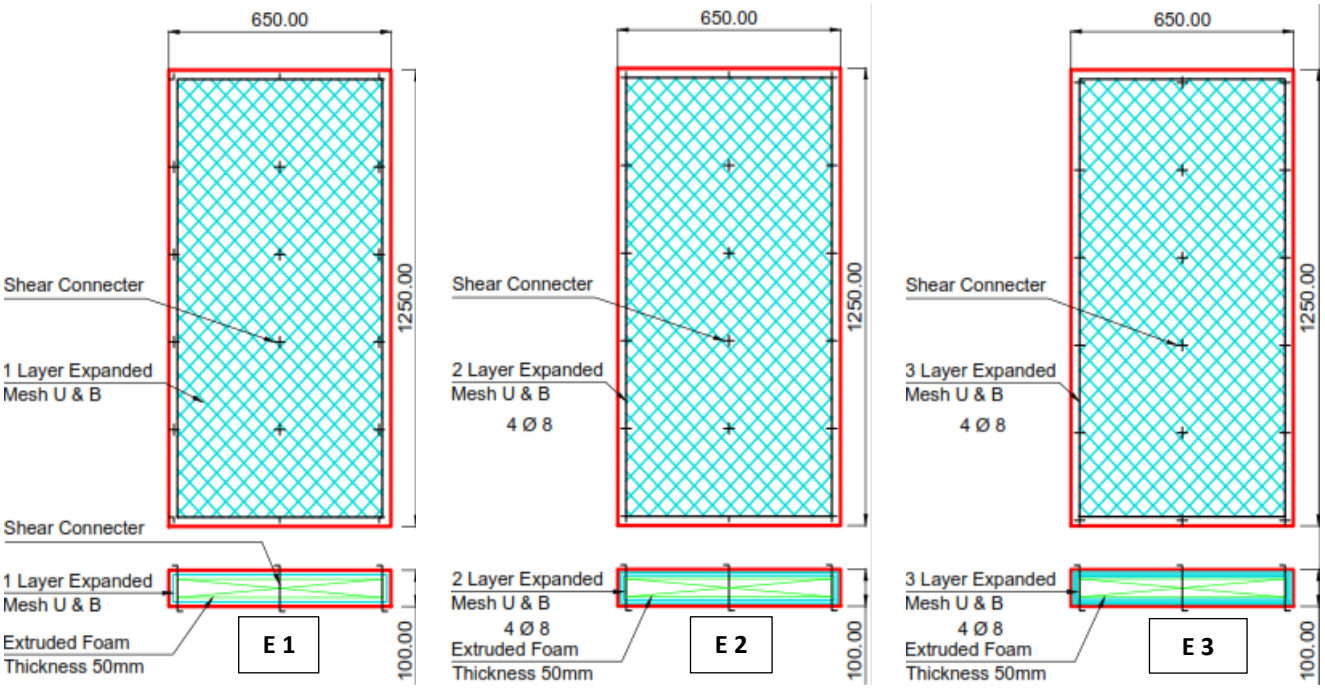

Fig. 4. Reinforcement details of Group-3 walls (E1, E2 and E3).

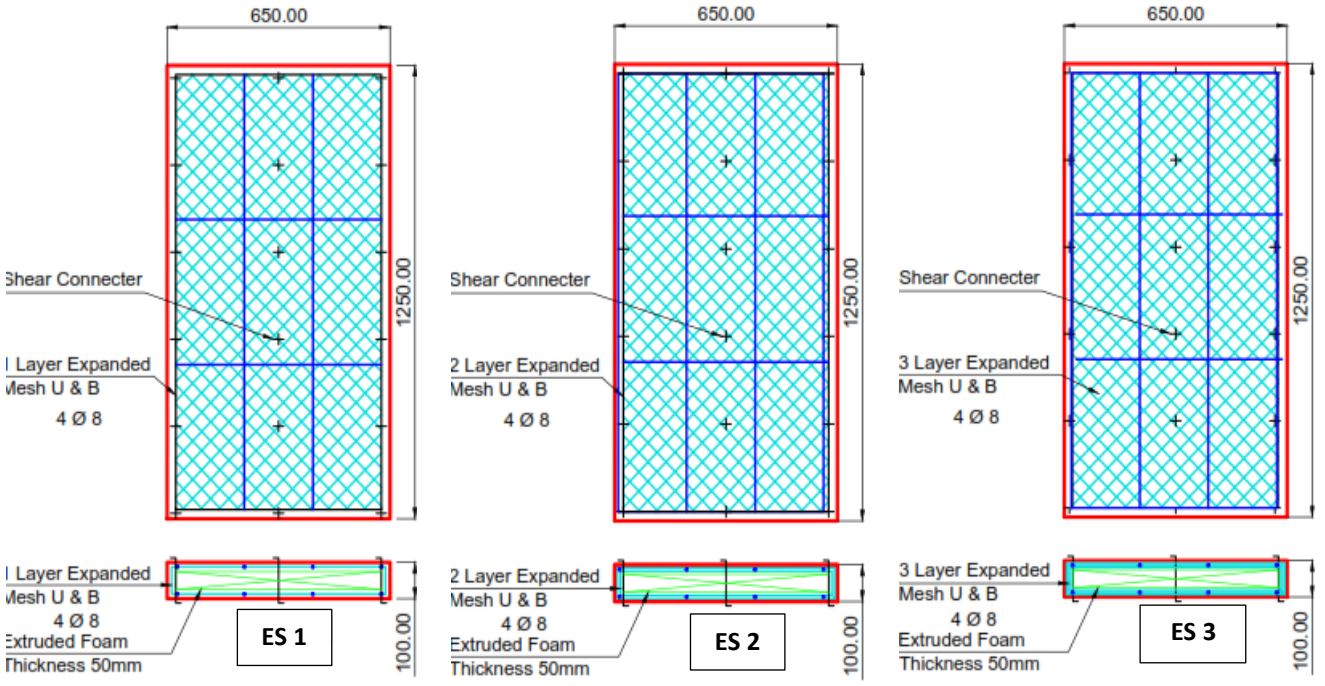

Fig. 5. Reinforcement details of Group-4 walls (ES1, ES2 and ES3).

4.2. Preparation of the reinforcement

There were some photo of preparation of reinforcement details of walls.

4.3. Design mix

The concrete mortar which was used of casting specimens was designed to have an ultimate compressive strength of 35 MPa after 28 days. The mortar matrix mix characteristics were determined using the ACI Committee 549 Report (1988). It was content of initially dry mixed before adding water and remixing the entire patch in the mixer. For all specimens, mechanical compaction was used. Table 5 shows the mix proportions by (kg\m^3). 15 cubes; 150 ×150 ×150 mm were cast and tested to determine the compressive strength of the mix at 7 and 28 days according to E.S.S. (2011).

Fig. 6. Preparation of the reinforcement.

Table 5. Mix design of the ferrocement mortar mix.

Component	Portland cement	Sand	Silica fume	Water	Super plasticizers	Polypropylene 300−e3
Amount (kg/m^3)	650	1300	65	227	6.5	0.9

The walls were installed by arranging the reinforcement. The reinforcements were then put in the molds. Then, the mortar was mixed by combining the sand and cement in dry form, then adding polypropylene fiber mesh after that, adding the slurry (silica fume, water and super plasticizer).

The whole mixing time was around 10 minutes, which was sufficient to produce a homogenous mixture. The mixture was then poured into the wooden shape. The walls were meticulously compressed to achieve complete compaction. After the molds were filled with concrete, the surface of the concrete in the molds was smoothed using a trowel. Finally, the walls were kept in the forms for 24 hours in laboratory settings before being scraped away.

4.4. Casting of concrete mix

Fig. 7 shows the photo for casting of concrete.

Fig. 7. Casting of concrete mix.

4.5. Test set-up

Four LVDT were mounted to follow the vertical and horizontal displacement, three displacement transducers (type P1) with gauge lengths of 200 mm, two were mounted in the middle of the front face and the third in the side face of the test specimen. All test specimens were tested to failure under concentric loadings at the wall ends. Loading Cells, and Testing Frame are the key components of the testing facility.

The force was added progressively with increments ranging from 5.0 to 20 kN for all test specimens, and once the vertical load reached 5 kN, the horizontal load was gradually applied, as indicated in Fig. 8(a,b). At all loading phases, all deformation properties, cracking patterns, and strengths were comprehensively measured. The walls were progressively loaded at two spots through a loading steel beam. As a result, the wall was loaded up to failure in stages. A load cell with a capacity of 3500 kN was used to measure the load on the wall. Following each loading phase, the vertical mid-span deflections (V1), vertical side deflections (V2), horizontal displacement (H1), Pi-gauge readings, and generated normal stresses were recoded and recorded using an automated data logger device (TDS-150). Tanta University's reinforced concrete and heavy structures lab.

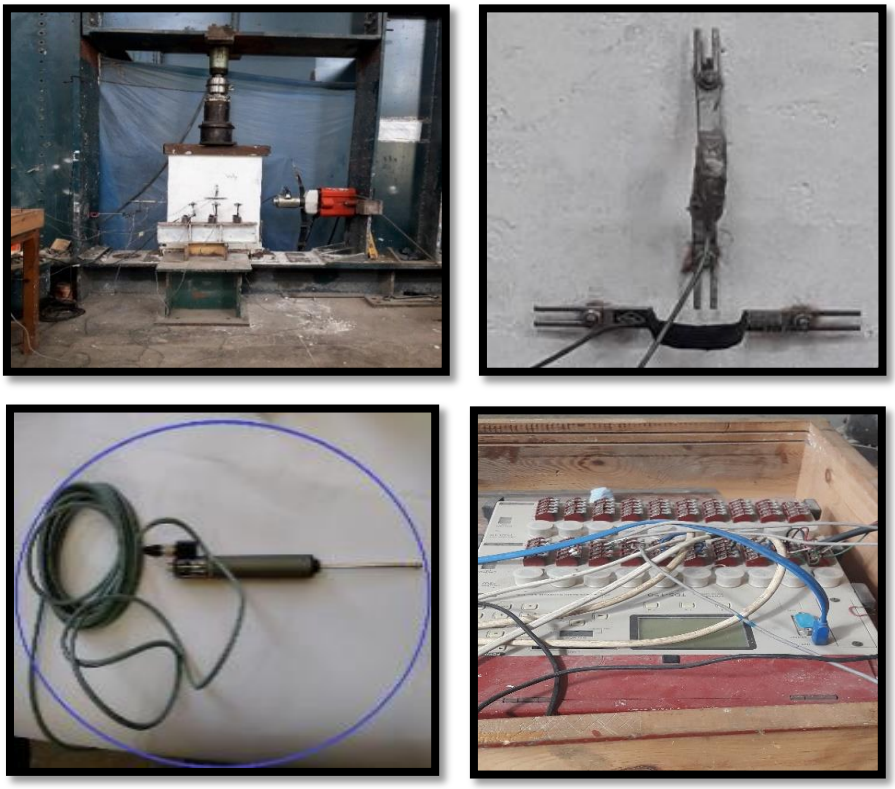

Fig. 8(a). Test set up and data logger unit used for the tests (TDS-150).

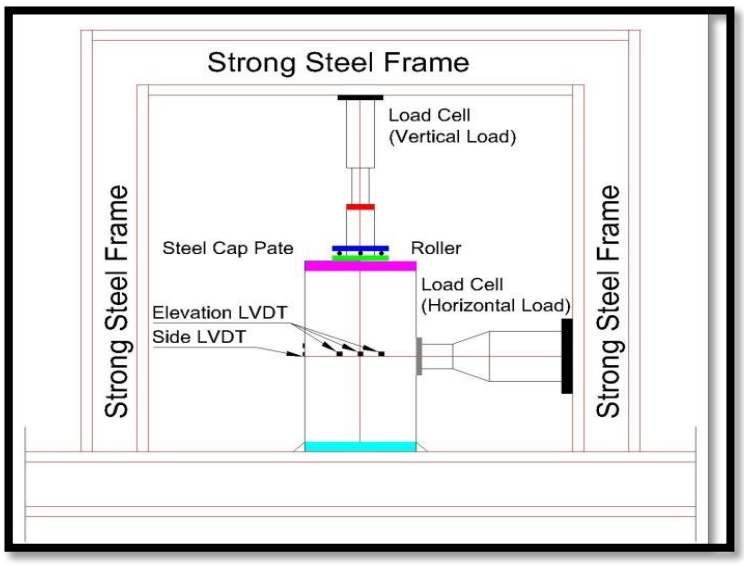

Fig. 8(b). Test set up in the vertical and horizontal loading test.

5. Experimental Results and Discussions

The findings for the initial loading, service load, vertical and horizontal displacement at ultimate load, ductility ratio, and energy absorption are shown in the Table 6. The first fracture load was calculated from the load deflection curve at the point when it began to depart from the linear relationship. The area under the load-deflection curve is sometimes used to define energy absorption. Figs. 9 and 10 show the first crack load and ultimate load.

5.1. Serviceability load

The serviceability load was computed using the CP110 equation: service load = (Experimental load - 1.4 D.L)/1.6 where the experimental load equals the greatest load achieved as shown in Fig. 11.

5.2. Ductility ratio

The ductility proportion was assessed by comparing the extreme stack mid-height uprooting to the starting breaking loads. When compared to divider CO, dividers fortified with extended metal work and welded steel work had a more prominent ductility proportion. Fig. 12 depicts the ductility proportions for all light weight dividers assessed.

5.3. Energy absorption

The energy absorption was calculated by computing the area under the load displacement curve for each wall, Energy = $\int_{u}^{\Delta u} f(\Delta) d\,\Delta$.

Walls strengthened with expanded steel mesh absorbed more energy than the control wall CO. Fig. 13 stresses energy absorption for all walls examined. Higher ductility and energy absorption are extremely beneficial in dynamic applications.

Table 6. Experimental results of vertical loading test for shear walls.

Wall	First crack V load (kN)	Ultimate V load (kN)	Serviceability V load (kN)	First crack H load	Ultimate H load (kN)	First crack V displacement (mm)	Maximum deflection (mm)	Ductility ratio	Energy absorption (kN.mm)
CO	112	185.30	115.72	68.34	98	0.541	2.20	4.06	283.55
W2	123	169.18	105.68	30	41	0.652	1.37	2.10	156.54
W3	133	182.24	113.83	50	74	1.07	1.93	1.80	244.30
W4	146	196.86	122.97	66	81	1.33	2.31	1.73	295.98
WS2	161	210.12	131.22	77	109	1.18	2.34	1.98	352.73
WS3	174	225.41	140.78	89	123	1.23	2.23	1.81	321.68
WS4	190	240.84	150.42	89	150	1.42	2.57	1.80	453.08
E1	143	190.77	119.15	72	95	1.24	2.17	1.91	315.86
E2	171	226.10	141.22	78	111	1.45	2.41	1.64	387.71
E3	180	230.18	143.77	80	115	1.72	2.64	1.30	413.87
ES1	181	250.24	156.30	50	105	1.54	2.57	1.72	427.96
ES2	209	287.30	179.44	52	144	2.02	3.35	1.62	703.63
ES3	241	290.35	181.33	64	155	2.42	4.43	1.48	922.47

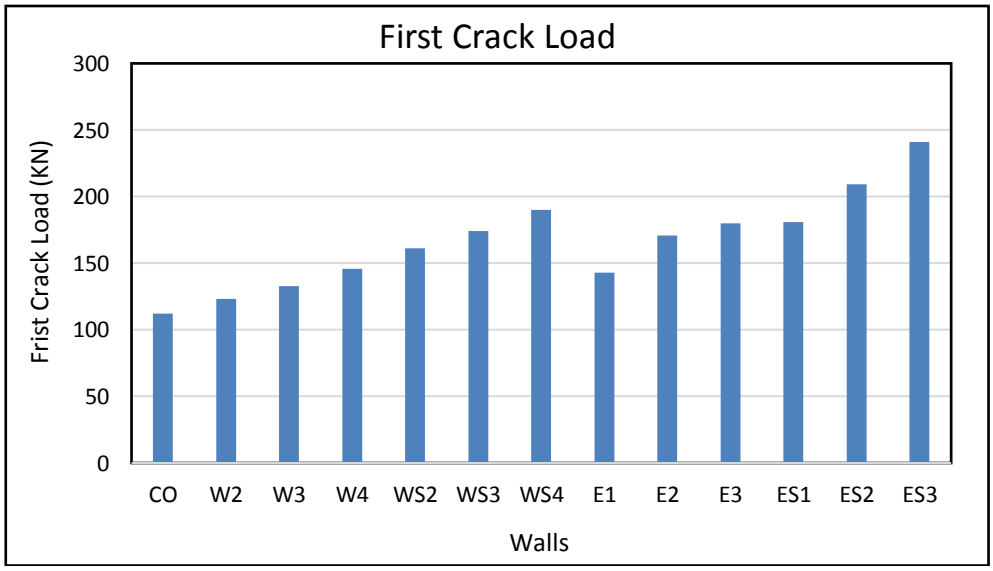

Fig. 9. First crack of tested of tested walls under vertical and horizontal loading.

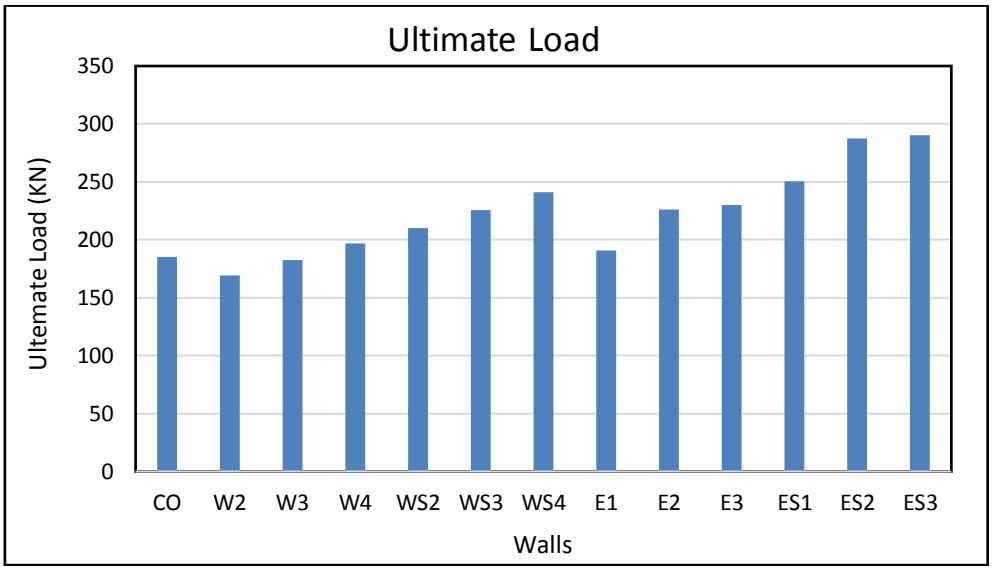

Fig. 10. Ultimate load of tested walls under vertical and horizontal loading.

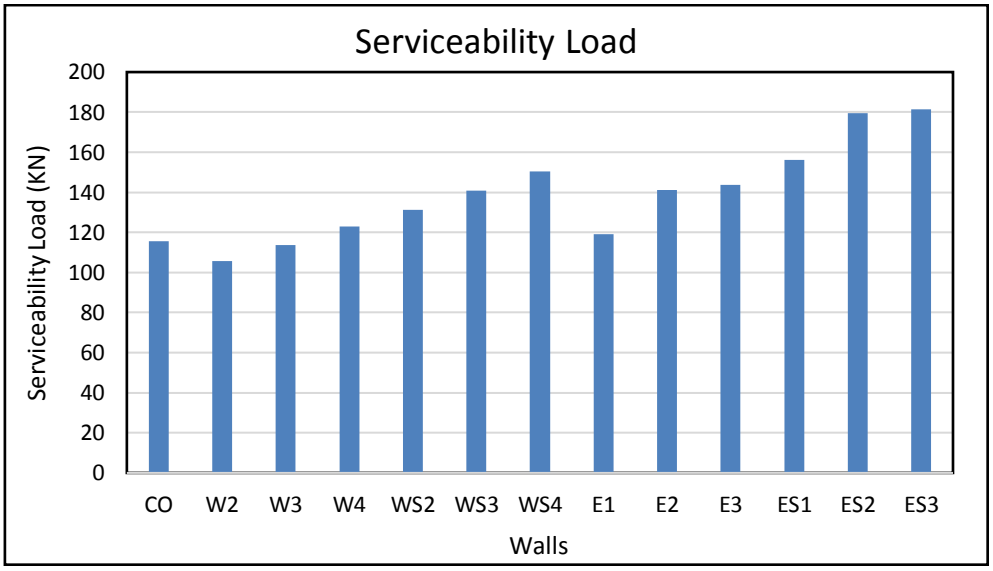

Fig. 11. Serviceability load of tested walls under vertical and horizontal loading.

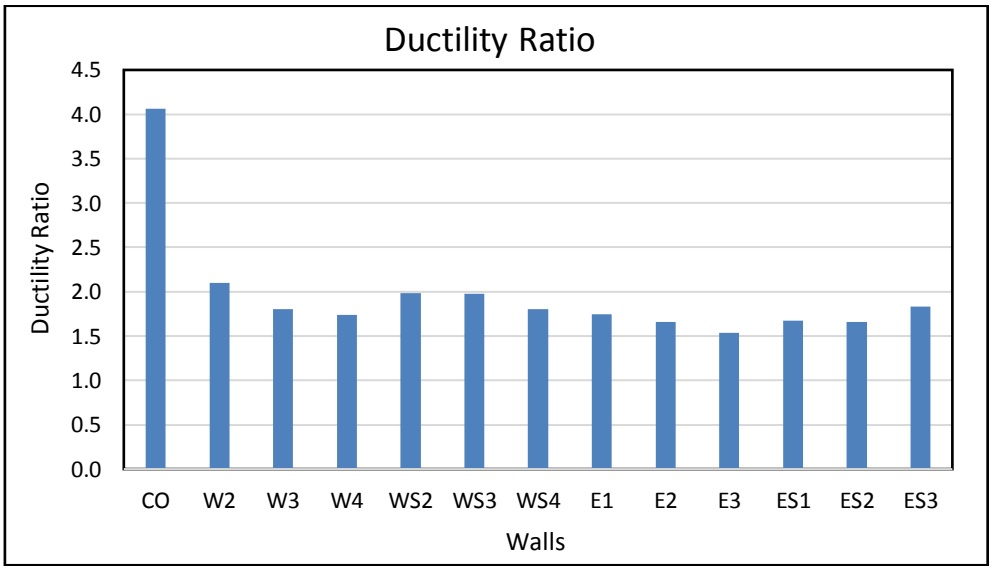

Fig. 12. Ductility ratio of tested walls under vertical and horizontal loading.

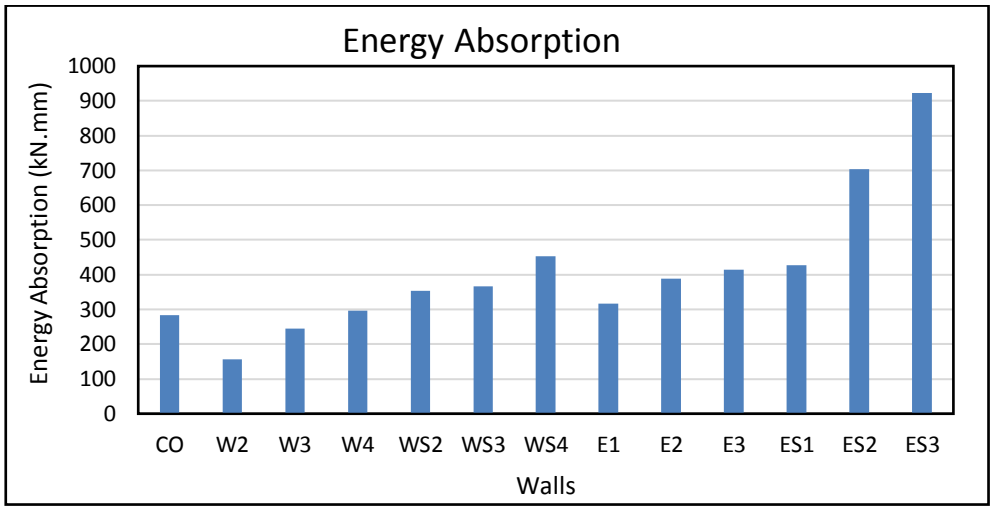

Fig. 13. Energy absorption of tested walls under vertical and horizontal loading.

5.4. Effect of type of reinforcement

Figs. 9, 10 and 13 depict the influence of several forms of reinforcement on the behavior of the tested walls. According to these results, the loads for control wall reinforcement with steel alone were the lowest when compared to walls reinforced with steel wire mesh alone or with steel wire mesh plus steel reinforcement. However, the energy absorption for walls reinforced with steel wire. meshes is higher than that for walls reinforced with steel reinforcement by 4%, 60%, 45%, &d 225% W4, WS4, E3, & ES3, respectively, when compared to CO.

Furthermore, as compared to CO, the ultimate load rose by 5%, 29%, 24%, & 56% for W4, WS4, E3 and ES3, respectively. When compared to CO, the first fracture load rose by 30%, 69%, 60%, & 115% for W4, WS4, E3 and ES3, respectively.

5.5. Effect of number of layer of reinforcement

Figs. 14-16 indicate the influence of the number of steel wire mesh layers. The initial cracking, maximum load, and energy absorptions increased as the quantity of welded steel wire mesh increased. In the case of welded steel mesh reinforced walls, the initial cracking load increased by 8% & 18% for three and four steel wire mesh layers (W3, W4) compared to two wire mesh layers, ultimate load increased by 7% and 12% for three and four steel wire mesh layers (W3, W4) compared to two wire mesh layers, and energy absorption increased by 62% and 96% for three and four steel wire mesh layers (W3, W4) compared to two wire mesh layers.

The initial cracking, ultimate load, and energy absorptions increased as the number of expanded steel wire mesh increased. In the case of walls reinforced with expanded steel mesh, the initial cracking load increased by 19% & 25% for two and three steel wire mesh layers (E2, E3) compared to one wire mesh layer, the ultimate load increased by 18% and 21% for two and three steel wire mesh layers (E2, E3) compared to one wire mesh layer, and energy absorption increased by 22% and 31% for two and three steel wire mesh layers (E2, E3) compared to one wire mesh layers.

5.6. Effect of presence of steel bars

Figs. 14-17 indicate the effect of the presence of steel bars with wire mesh. The first cracking, maximum load, and energy absorptions of the walls increased as the walls were strengthened with welded steel wire mesh and steel bars. The first cracking load rose by 30%, 28%, and 30% for walls reinforced with welded steel mesh and steel bars (WS2, WS3 and WS4), respectively, as compared to walls reinforced with welded steel mesh only (W2 ,W3 and W4),

Ultimate load increased by 24%, 23%, and 26% for walls reinforced with welded steel mesh with steel bars (WS2, WS3, and WS4) compared to walls reinforced with welded steel mesh only (W2,W3 and W4), and energy absorption increased by 134%, 131%, and 153% for walls reinforced with welded steel mesh with steel bars (WS2, WS3 and WS4).

The first cracking, maximum load, and energy absorptions of the walls increased as the walls were strengthened with expanded steel wire mesh and steel bars. When compared to walls reinforced with welded steel mesh only, the first cracking load rose by 26%, 22%, and 33% for walls reinforced with expanded steel mesh with steel bars (ES1, ES2 and ES3) (E1 ,E2 and E3), ultimate load increased by 31%,26%, and 26% for walls reinforced with expanded steel mesh with steel bars (ES1, ES2 and ES3) compared to walls reinforced with expanded steel mesh only (E1 ,E2 and E3), and energy absorption increased by 35%,81%, and 123% for walls reinforced with expanded steel mesh only.

5.7. Effect of using various types of meshes

Figs. 18-21 demonstrate the effect of employing different types of meshes. When a wall was reinforced with two layers of welded steel wire mesh against a wall reinforced with two layers of expanded steel wire mesh (W2, E2), the first cracking, maximum load, and energy absorptions increased. The initial cracking load rose by 39%, the maximum load by 24%, and energy absorption by 185%. When a wall was reinforced with three layers of welded steel wire mesh against a wall reinforced with

three layers of expanded steel wire mesh (W3, E3), the first cracking, maximum load, and energy absorptions increased. The initial cracking load rose by 35%, the maximum load by 26%, and energy absorption by 69%. Similarly, by reinforcing with various types of wire meshes and steel bars), the initial cracking, maximum load, and energy absorptions are increased as reported by Shaheen et al. (2023).

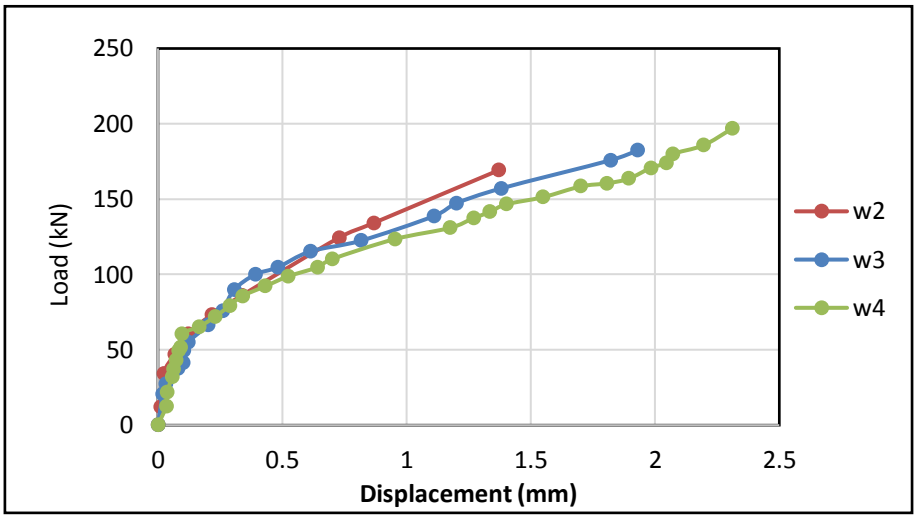

Fig. 14. Load-vertical displacement for Group-1.

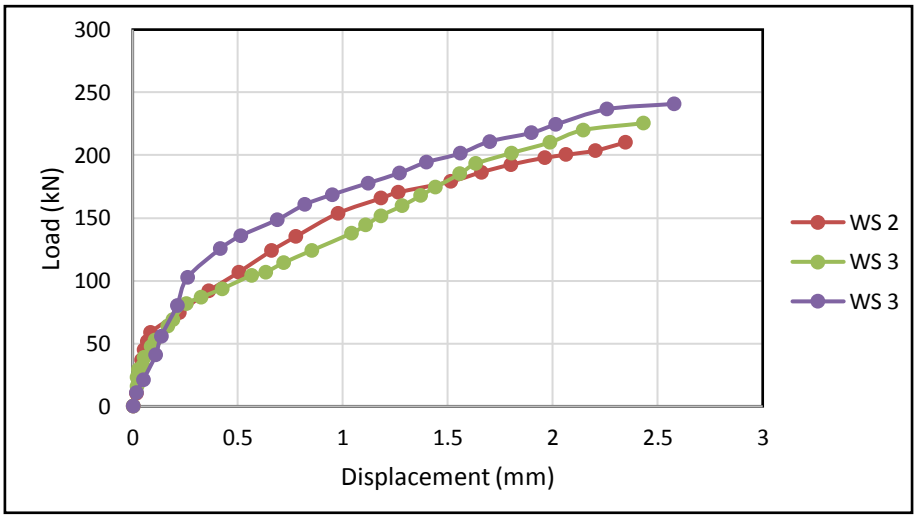

Fig. 15. Load-vertical displacement for Group-2.

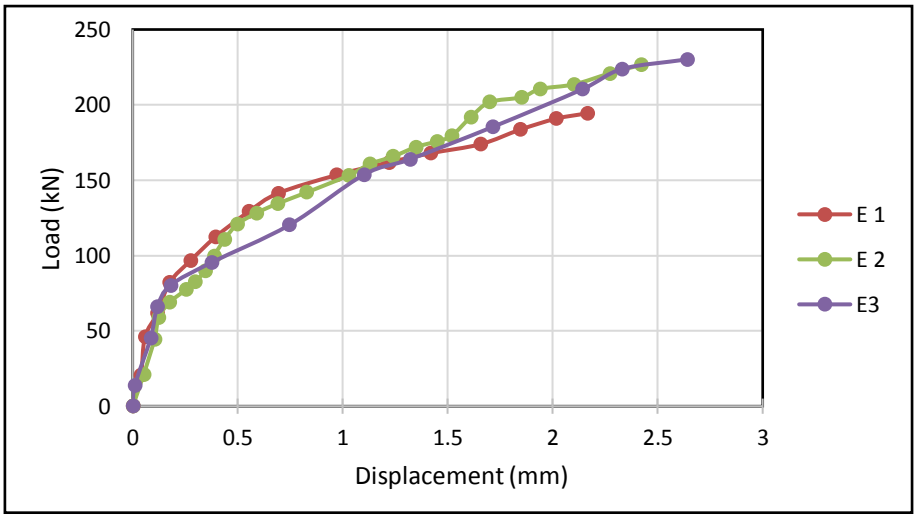

Fig. 16. Load-vertical displacement for Group-3.

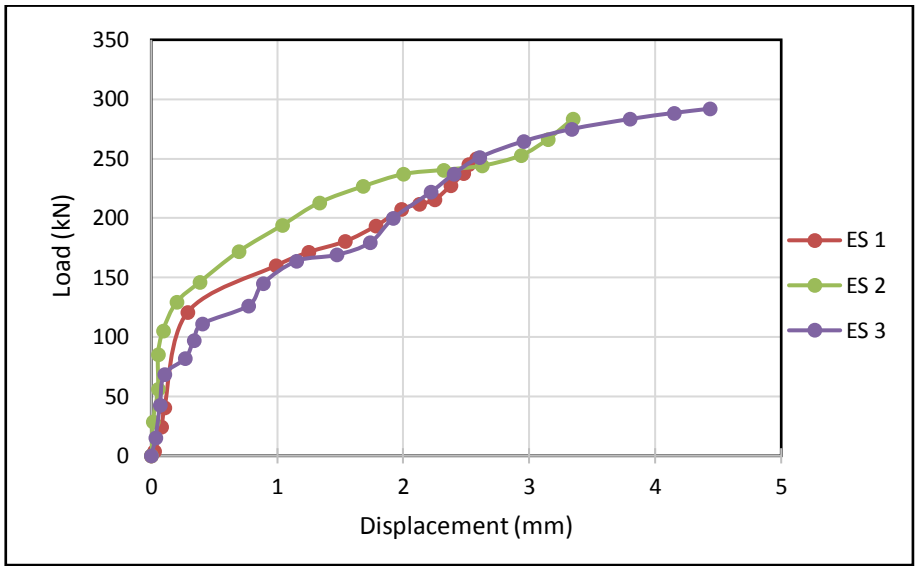

Fig. 17. Load-vertical displacement for Group-4.

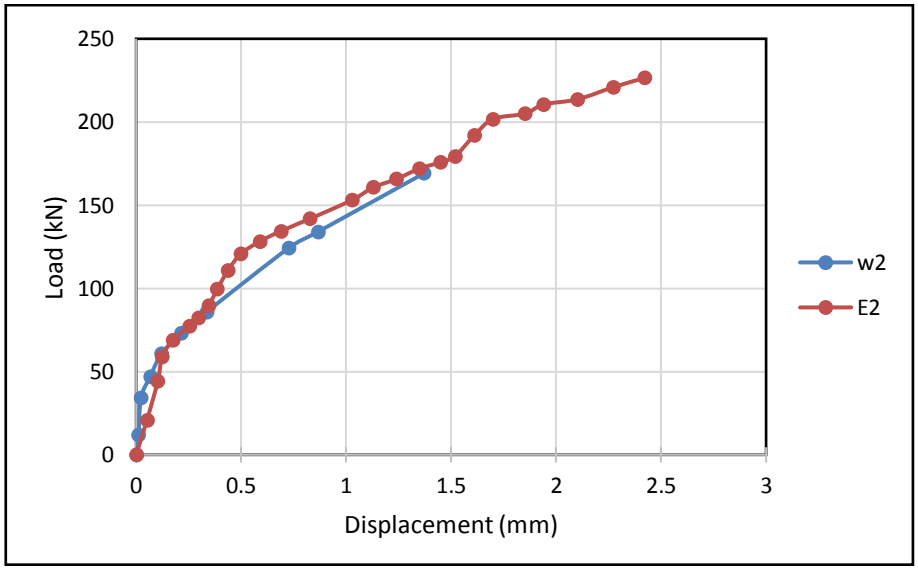

Fig. 18. Load-vertical displacement for W2 and E2.

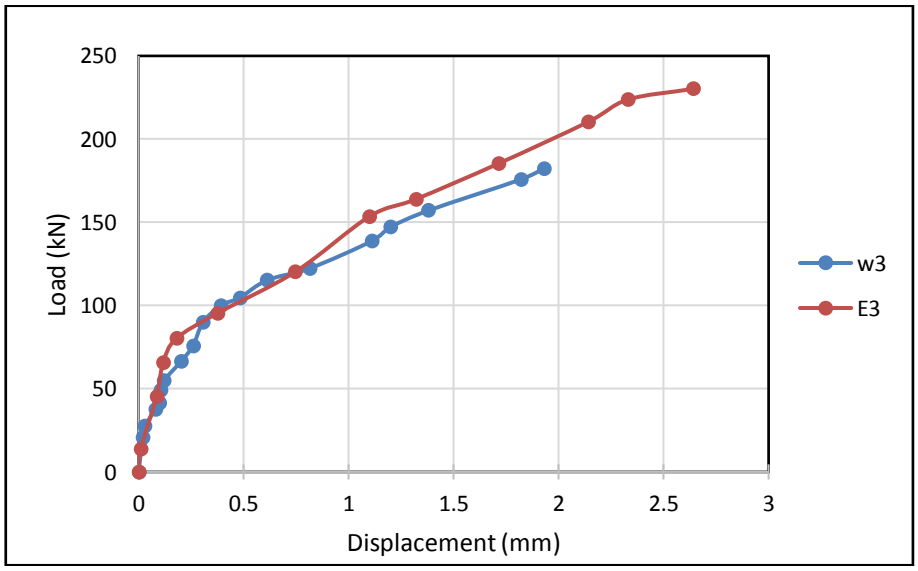

Fig. 19. Load-vertical displacement for W3 and E3.

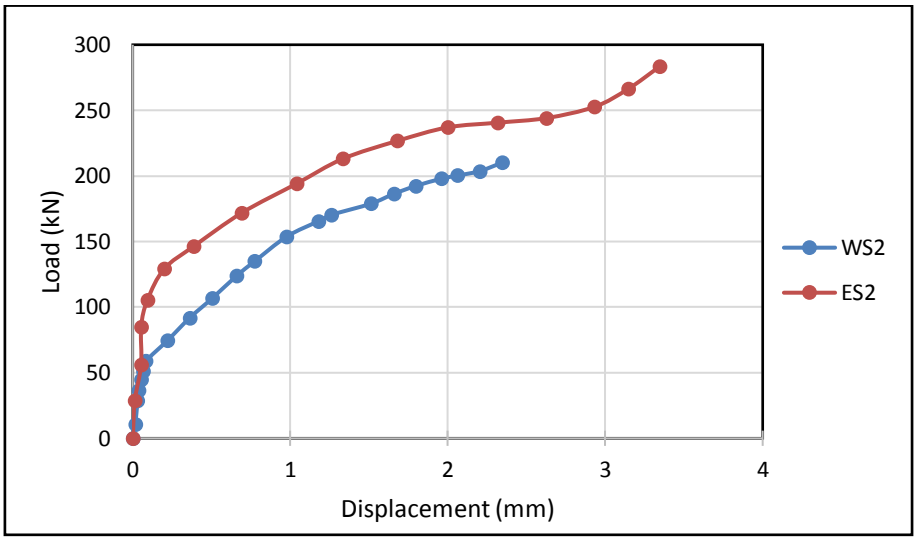

Fig. 20. Load-vertical displacement for WS2 and ES2.

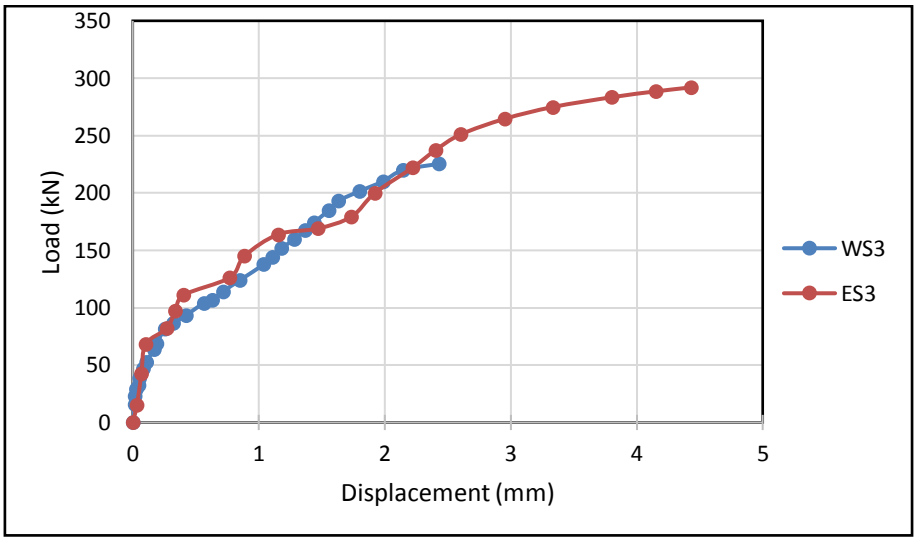

Fig. 21. Load-vertical displacement for WS3 and ES3.

5.8. Load-strain relationship

The load-strain curves for all tested walls were shown in Figs. 22-26 for all walls, the relationship among the load and strain was almost linear till the first crack load then it started to deviate from the linear relation.

5.9. Cracking behavior

Fig. 27 shows cracking patterns of all the tested light weight walls subject to compression and lateral loadings. We can observe the function of specific surface area of reinforcing and the presence of mesh reinforcement, to control crack width.

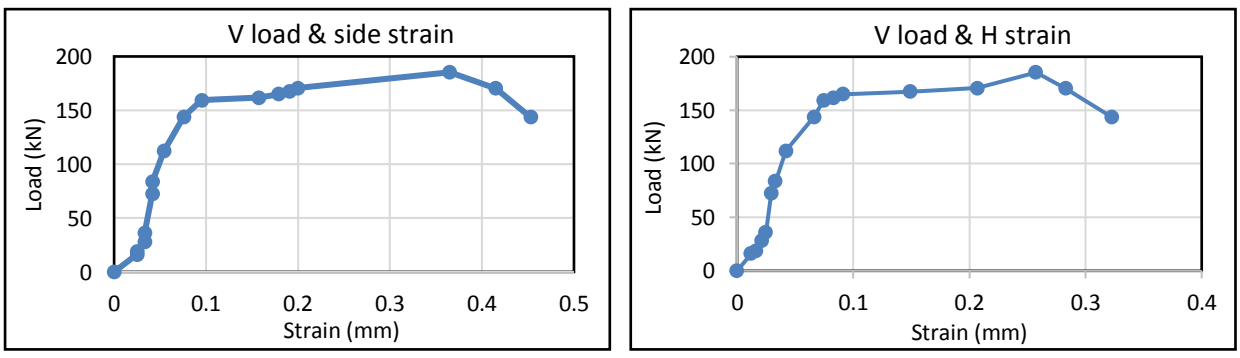

Fig. 22. Load-horizontal and -side strain for CO.

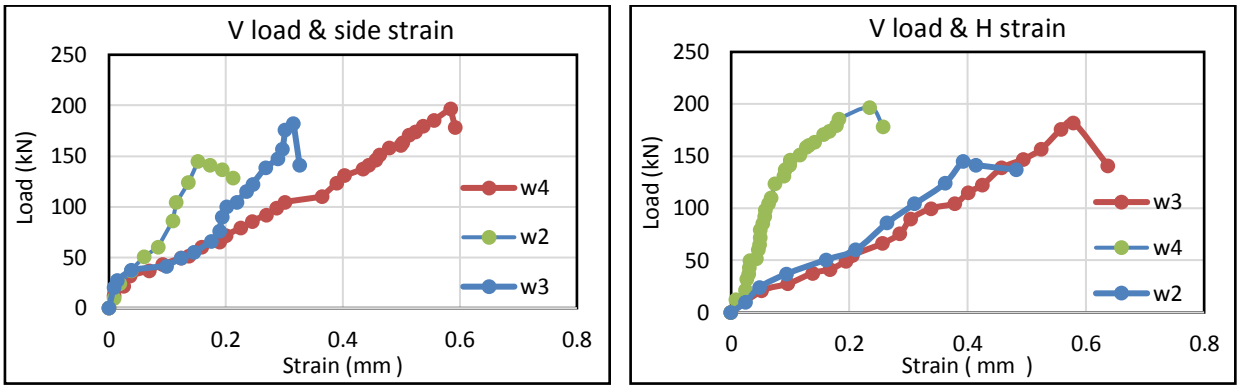

Fig. 23. Load-horizontal and -side strain for W2, W3 and W4.

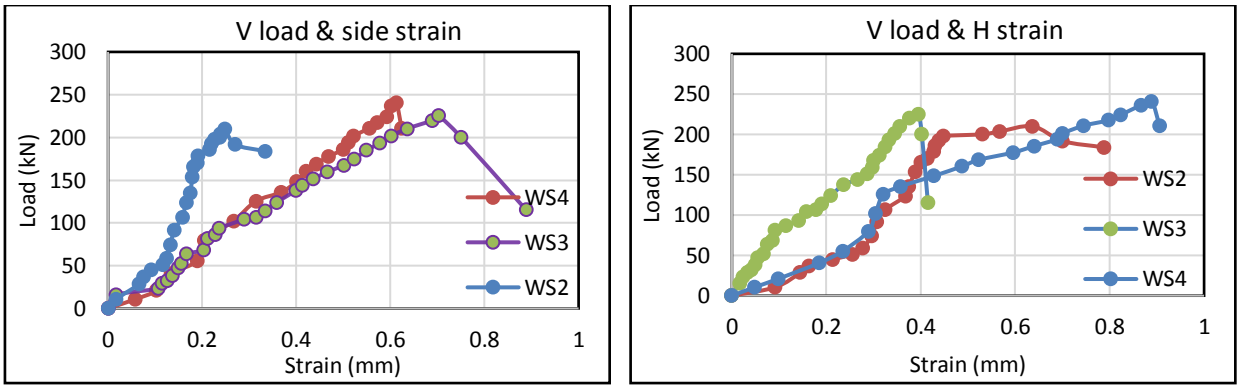

Fig. 24. Load-horizontal and -side strain for WS2, WS3 and WS4.

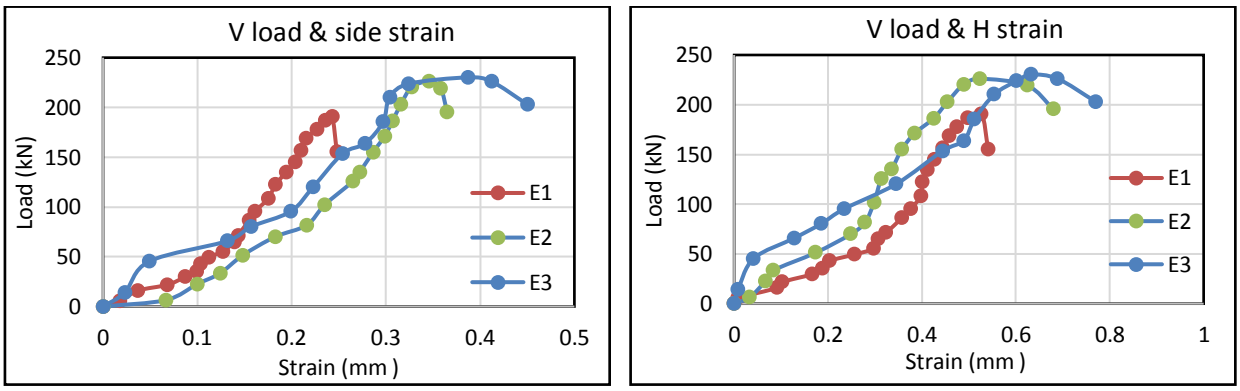

Fig. 25. Load-horizontal and -side strain for E1, E2 and E3.

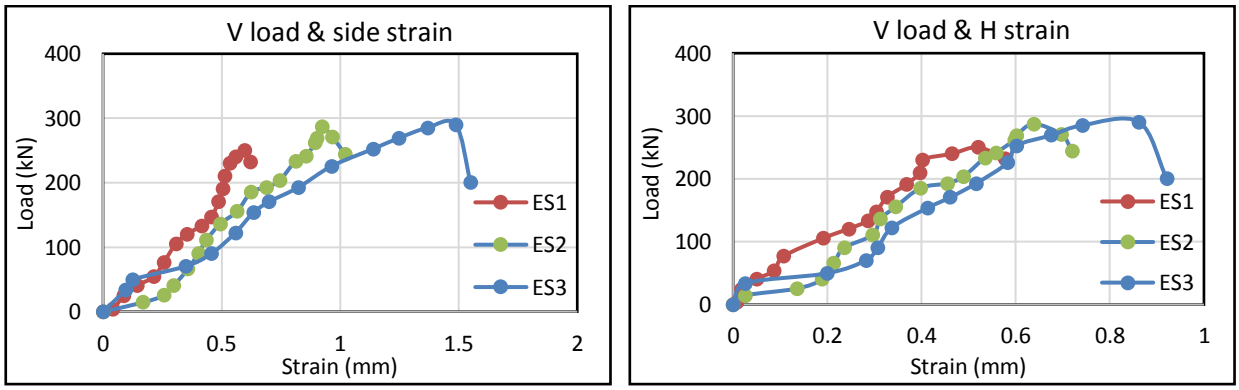

Fig. 26. Load-horizontal and -side strain for ES1, ES2 and ES3.

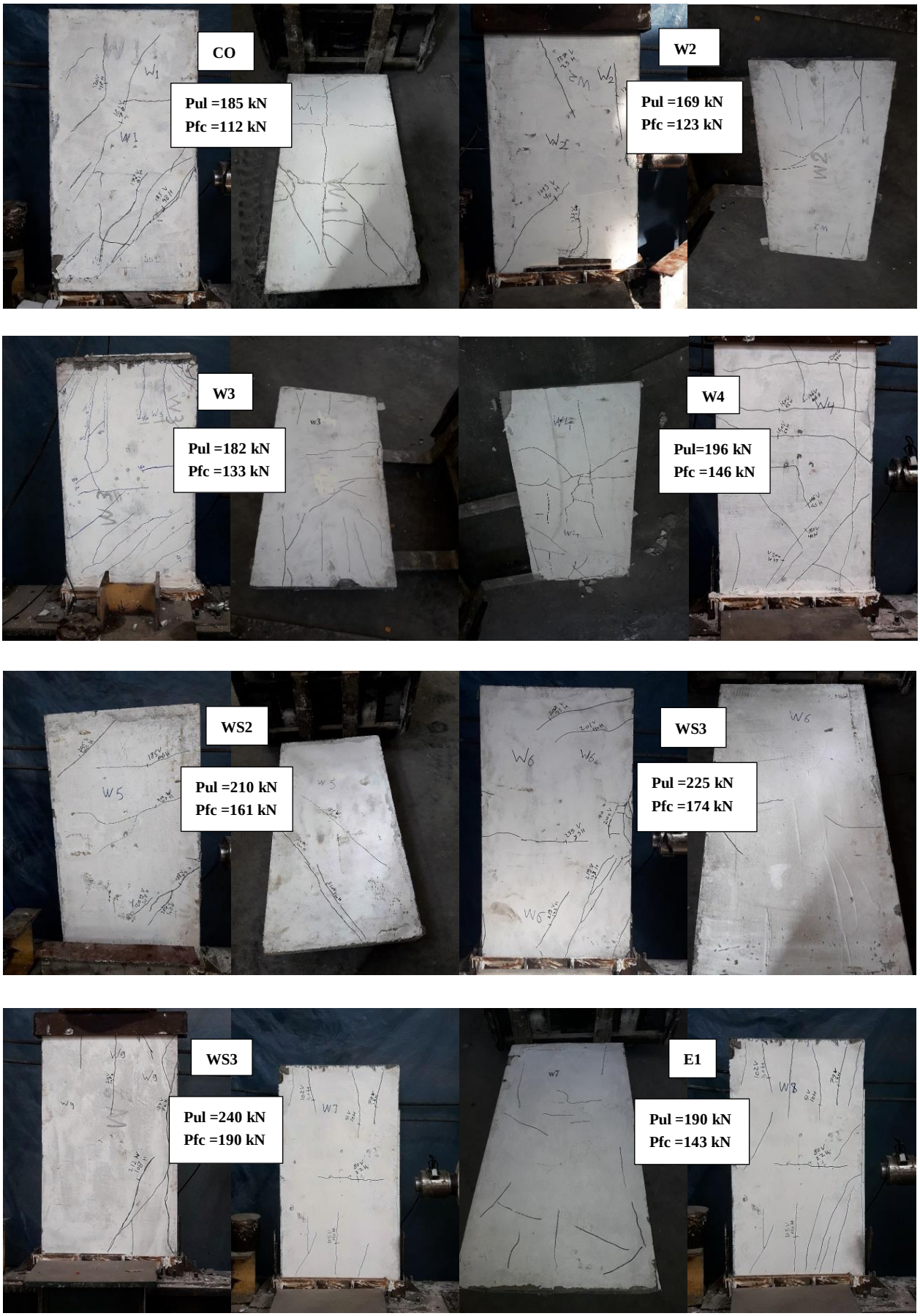

Fig. 27. (continued)

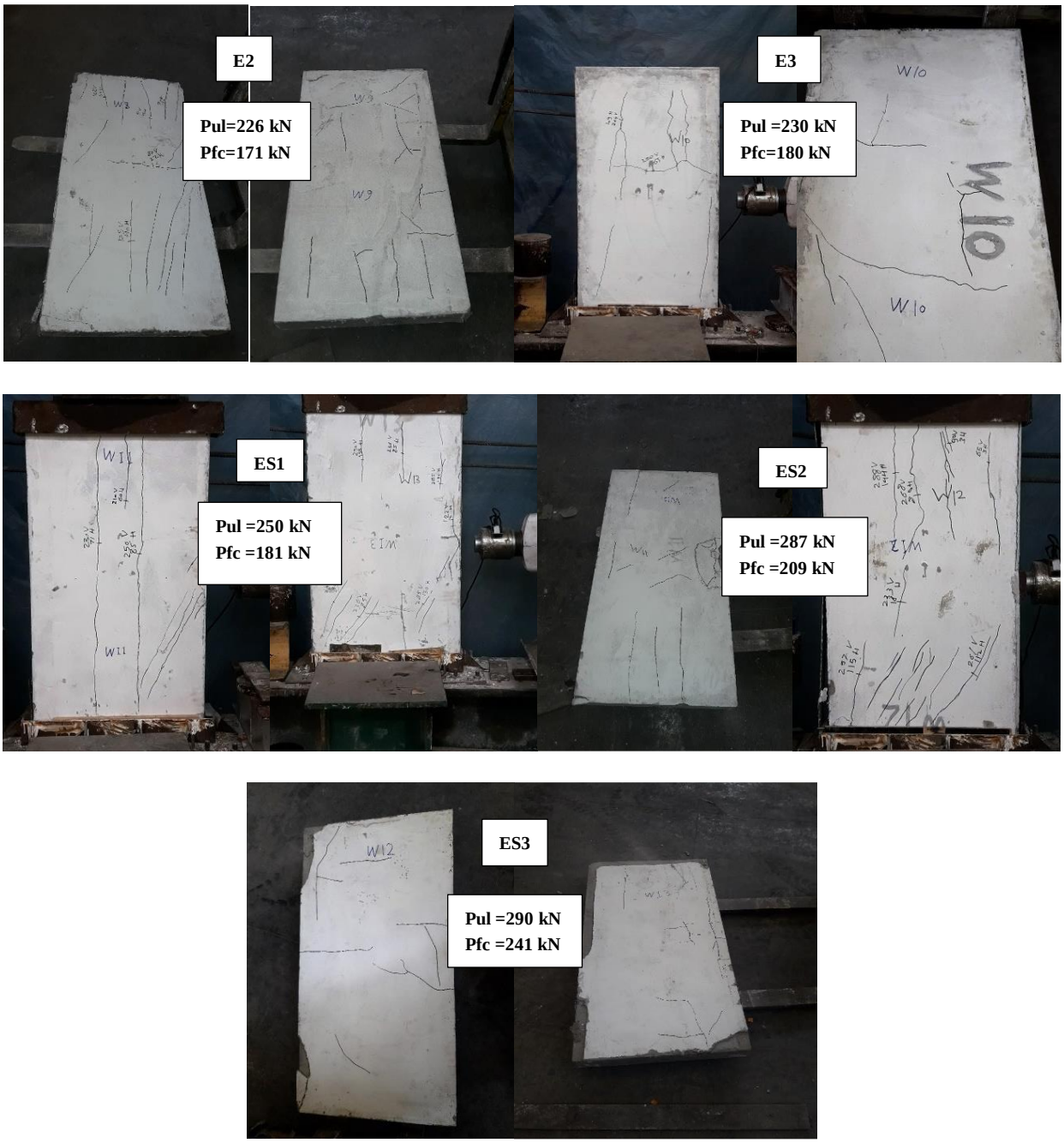

Fig. 27. Crack patterns of the wall.

5.10. Finite element model

A finite element package ABAQUS was used to emulate the performance of ferrocement walls as a nonlinear finite element analysis. This part consist of the initial cracking load, ultimate load, cracking pattern, stress distribution and displacement due to vertical load.

Two kind of elements were used; solid element and truss element. The SOLID 65 (C3D8R) is used to know and emulate the reinforced concrete, truss element (T3D2) is used to know the steel bar by two nodes. Tables 7-9 show the properties of concrete and steel. Fig. 28 displays geometrical model for simulated specimens.

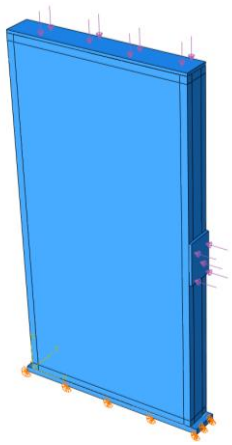

Fig. 28. Geometrical model for simulated specimens.

Table 7. Elastic properties of concrete.

Parameter	Value
Density	2.4×10-9 N/mm³
Mod. of elasticity	21900 MPa
Poisson's ratio	0.168

Table 8. Concrete plasticity parameters.

Parameter	Value
Dilation angle	42
Eccentricity	0.11
f_b/f_c	1.35
K	0.68
Viscosity parameter	0.0001
Yield stress in compression	17 MPa
Cross bonding inelastic strain	0.00
Compressive ultimate stress	33 MPa
Cross bonding inelastic strain	0.00158
Tensile failure stress	3.45 MPa

5.11. Boundary condition

The loads were reacted as pressure on contact area which was (100×650 mm) for compressive load and was (100×100 mm) for side load. The bottom surface of concrete wall was installed to be fixed to prevent from translation XZ, XY, YZ directions and from rotation about XY direction at the two lines of contact with underneath roller supports.

5.12. Finite element results compared with experimental results

The findings of the ferrocement walls were compared with theoretical results and the experimental results. The load-displacement curves for all tested specimens were displayed in figures and have an excellent agreement between theoretical and experimental results as shown in Fig. 29 and Table 10.

Table 9. Elastic properties of steel bars and metal meshes.

Steel 24/35		Welded mesh		Expanded mesh	
Density		Density		Density	
7.86×10-9		7.86×10-9		7.8×10-9	
Mod. of elasticity	Poisson's ratio	Mod. of elasticity	Poisson's ratio	Mod. of elasticity	Poisson's ratio
205000	0.3	170000	0.28	130000	0.28
Stress	Strain	Stress	Strain	Stress	Strain
240	0	413	0.00	199	0
350	0.0951	610	0.05763	320	4.95E-02

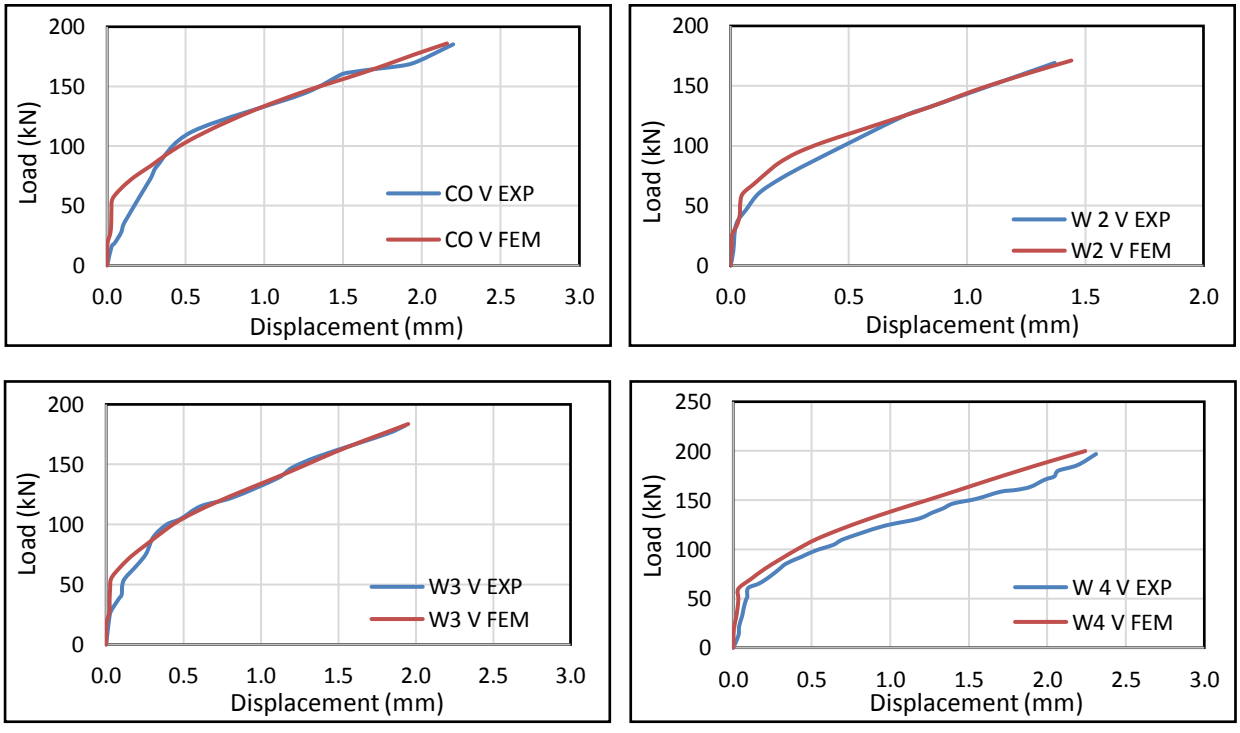

Fig. 29. (continued)

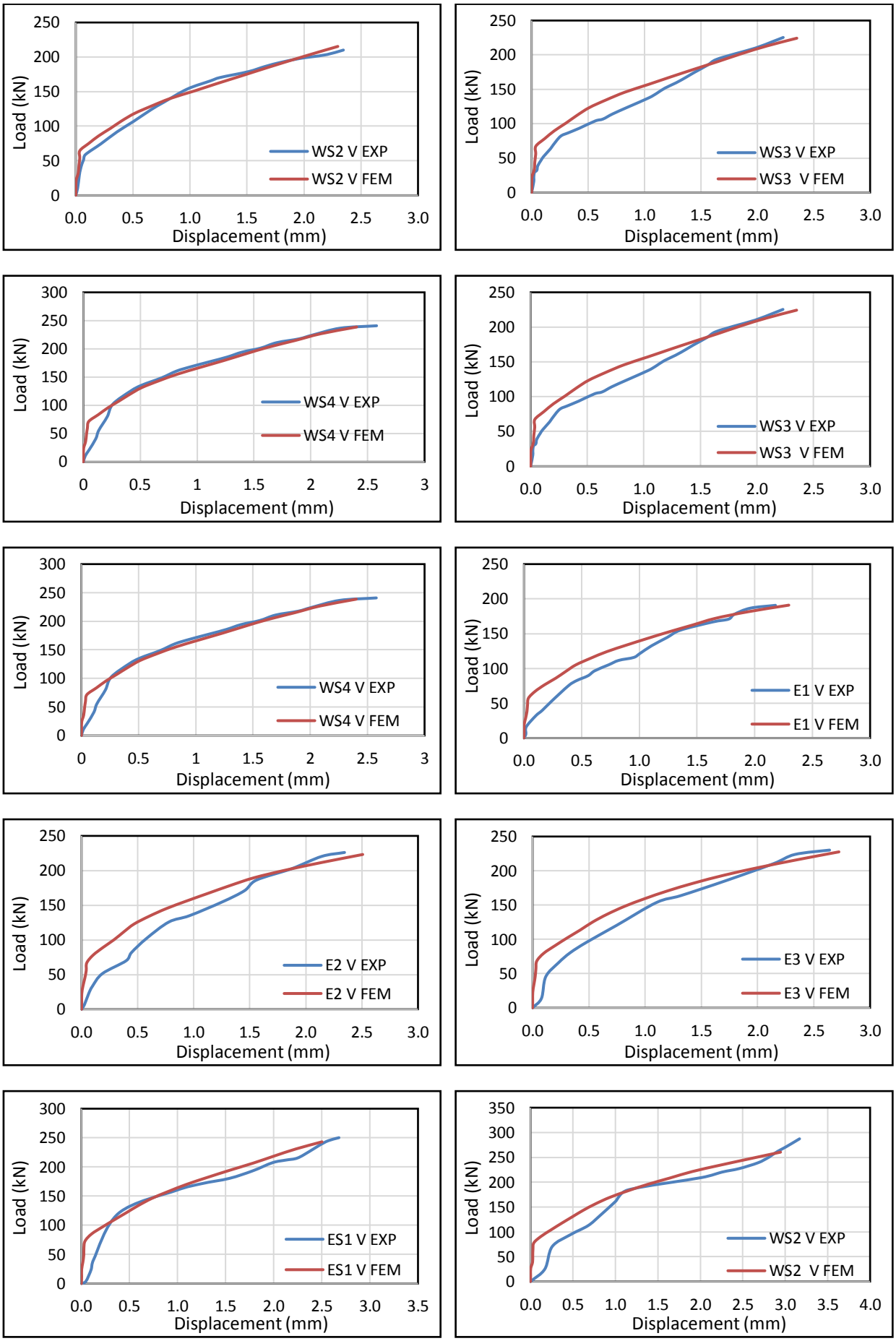

Fig. 29. (continued)

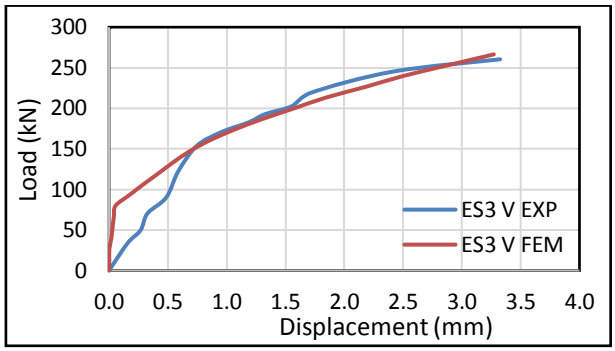

Fig. 29. Comparison between experimental and finite element.

Table 10. Comparison between the results the theoretical and experimental results.

Wall	First crack load (kN)		Ultimate load (kN)		P_{fc} FEM/Exp.	P_{ut} FEM/Exp.
	Exp.	FEM	Exp.	FEM		
CO1	112	148.8	185.3	186.0	1.329	1.004
W2	123	162.6	169.2	171.2	1.322	1.012
W3	133	174.5	182.2	183.6	1.312	1.008
W4	146	179.9	196.9	199.9	1.232	1.015
WS5	161	161.5	210.1	215.4	1.003	1.025
WS3	174	168.2	225.4	224.4	0.967	0.995
WS4	190	179.0	240.8	238.7	0.942	0.991
E1	143	143.3	190.8	191.0	1.002	1.001
E2	171	145.1	226.1	223.2	0.848	0.987
E3	180	159.3	230.2	227.6	0.885	0.989
ES1	181	145.9	250.2	243.1	0.806	0.971
ES2	209	156.23	287.3	260.5	0.748	0.907
ES3	241	159.9	290.4	266.4	0.663	0.918

6. Conclusions

The following conclusions could be formed as follows:

- The ultimate load and rose by 7 and 12% for specimens with three and four layers of steel mesh, respectively, as compared to the wall with two layers of welded steel mesh and energy absorbed increased by 62 and 96%.
- The ultimate load rose by 18 and 21% for specimens with two and three layers of steel mesh, respectively, as compared to the wall with one layer of expanded steel mesh and energy absorbed increased by 22 and 31%.
- Increasing the reinforcing volume percent improved the first fractures, ultimate loads, and energy absorption means increase number of layers meshes reinforcement.
- For the walls reinforced with expanded mesh, the ultimate load was greater than the walls reinforced with welded mesh by 22% and energy absorbed increased by 53%.
- Excellent agreement among theoretical and experimental results.
- Out of this research, using these walls low cost, light weight and can use as precast elements.

It is also suggested to investigate the behavior of the proposed system under impact and dynamic loadings and earth quick load.

Acknowledgements

None declared.

Funding

The authors received no financial support for the research, authorship, and/or publication of this manuscript.

Conflict of Interest

The authors declared no potential conflicts of interest with respect to the research, authorship, and/or publication of this manuscript.

REFERENCES

ACI 213R-87 (1999). Guide for structural lightweight aggregate concrete. ACI manual of concrete practice, American Concrete Institute, Detroit.

ACI 549-R97 (2009). State-of-the-art report on ferrocement. ACI manual of concrete practice, American Concrete Institute, Detroit.

ASTM C494/C494M (2001). Standard specification for chemical admixtures for concrete. ASTM International, West Conshohocken, PA.

ASTM C1116/C1116M-10a (2015). Standard specification for fiber reinforced concrete. ASTM International, West Conshohocken, PA.

Bhalsin S, Shoaib S, Autade P (2014). Tensile strength of ferrocement with respect to specific surface. *International Journal of Innovative Research in Science, Engineering and Technology,* 3(4), 501–507.

E.S.S 4756-11 (2013). Physical and mechanical properties examination of cement, Part 1. Egyptian Standards Specification, Cairo, Egypt.

ECP 203-2007 (2020). Design and construction for reinforced concrete structures. Egyptian Code of Practice: Ministry of Building Construction, Research Center for Housing, Building and Physical Planning, Cairo, Egypt.

Eltehawy E (2009). Effect of using ferro-cement on the mechanical properties of reinforced concrete slabs subjected to dynamic loads. *13th International Conference on Aerospace Science and Aviation Technology.*

Gaba H, Singh H (2008). The study of economy of ferrocement with fly ash as an admixture. *12th International Conference of International Association for Computer Methods and Advances in Geomechanics*.

Naaman AE (2000). Ferrocement and laminated cementitious composites. *Materials and Structures*, 33(1).

Shaheen YB, Eltehawy EA (2017). Structural behavior of ferrocement channels slabs for low cost housing. *Challenge Journal of Concrete Research Letters*, 8(2), 48-64.

Shaheen YBI, Etman ZA, Ramadan AG (2018). Characteristics of ferrocement lightweight wall. *International Journal of Civil Engineering*, 16(1).

Shaheen YBI, Etman ZA, Gomaa O (2019). Structural behavior of thin ferrocement plates with and without stiffeners subjected to compression loading. *Asian Journal of Civil Engineering,* 20, 237–260.

Shaheen YBI, Etman ZA, Marzouk LA (2021). Bending behavior of ferrocement composite semicircular light weight panels for roof construction. *Journal of Materials Science Research and Reviews,* 8(4), 39-71.

Shaheen YBI, Refat HM, Mahmoud AM (2021). Structural behavior of concrete walls reinforced with ferrocement laminates, *Structural Engineering and Mechanics*, 78(4), 455-471.

Shaheen YBI, Etman ZA, Seyam AM (2022). Structural characteristics of lightweight ferrocement walls with various types of core materials and mesh reinforcement. *Current Journal of Applied Science and Technology*, 41(18), 15-45.

Shaheen YBI, Etman ZA, Elhosine NK (2023). Flexural behavior of lightweight ferrocement composite beams. *Advanced Engineering Technology and Application,* 2, 13-23.

Wafa MA, Fukuzawa K (2010). Characteristics of ferrocement thin composite elements using various reinforcement meshes in flexure. *Journal of Reinforced Plastics and Composites,* 29(23), 3530–3539.

Wang S, Naaman AE, Li VC (2004). Bending response of hybrid ferrocement plates with meshes and fibers. *Journal of Ferrocement,* 34(1), 275–288